V.G. LITOVCHENKO

V.E. Lashkaryov Institute of Semiconductor Physics, Nat. Acad. of Sci. of Ukraine
(41, Nauky Ave., Kyiv 03028, Ukraine; e-mail: lvg@isp.kiev.ua)

SURFACE PHOTOVOLTAGE SPECTROSCOPY RESEARCH OF SOLAR SILICON RECOMBINATION PARAMETERS

Fundamental recombination parameters of a photosensitive solar silicon material have been studied using the surface photovoltage spectroscopy. The method proposed is analyzed on the basis of photosensitive silicon structures of four types: industrial photosensitive Si wafers with the chemically etched (real) surface, structures with the implanted recombination-active Fe^+ impurity, SiO_2–Si structures with the surface-induced inversion channel, and structures with the diffused p–n junction. A comparison with the formulas obtained for the spectra of direct, V_{SC}, and inverse, $1/V_{SC}$, photovoltages in terms of the absorption coefficient k and its reciprocal quantity $1/k$ is carried out. The surface and bulk recombination rates and the distributions of recombination-active impurities, structural technological impurities, and defects in the near-surface charge region of solar silicon are calculated.

K e y w o r d s: surface photovoltage spectroscopy, solar silicon, near-surface charge region.

1. Introduction

Recombination parameters of the photosensitive Si material, as well as Si solar cells (SCs), have been studied earlier at a lot of various laboratories, in particular, with the use of photovoltage spectroscopy [1–11]. In modern SCs with front-side barriers, the surface recombination is reduced, owing to its screening by heavily doped thin layers, which form a recombination barrier for photo-induced charge carriers. The surface recombination turns out to be more critical in a number of other cases; namely, for novel "back side" SCs (with the Swenson design, with a multilayered structure, *etc.*), in which the illuminated surface barrier is strongly affected by the aging and other external factors. At the same time, the researches of near-surface regions in the corresponding devices, as well as in the solar Si material itself, are incomplete, in particular, concerning the influence of the doped surface layer, the defects inserted at the surface treatment, the energy and depth distributions of traps near the surface, the role of surface space charge, and so forth. In this work, the attention is focused on the consideration of the short-wave interval of photovoltage spectra, where the surface effects are the most pronounced.

2. Experimental Part

In order to obtain generalized conclusions, specimens of the following four types were studied.

1. *p*-Si wafers 400 μm in thickness with the chemically etched (CP-4) "real" surface, which was characterized by a relatively low density of surface states, $N_{ts} < 5 \times 10^{11}$ cm^{-2}, and a low surface recombination rate, $S \sim 10^2 \div 10^3$ cm/s.

2. The same material, but doped with Fe, by using the ion implantation technique, to the concentration $N_{ts} \sim 10^{15}$ cm^{-3} (see Fig. 1). Ion implantation was used to fabricate a specimen with a well-determined near-surface distribution of traps (an exposure dose of 10^{15} cm^{-3} and the ion energy $E_{ion} = 10^5$ V/cm).

3. The SC with a *p–n* junction formed by applying the standard technology of the thermal diffusion of donor impurities.

4. The SC with an induced surface channel (the Schottky layer) and covered with an Al grid contact prepared by the vacuum evaporation. In this case, the wafers were oxidized following the MIS technology at rather low temperatures (800–900°C) in order to avoid the growth of recombination losses and the bulk doping [8, 9]. The density of the surface charge built-in into the SiO$_2$ layer reached a magnitude of $(1 \div 5) \times 10^{12}$ cm$^{-2} \approx 10^{18}$ cm^{-3}, which gave rise to the formation of a rather large depletion or inver-

sion layer (the "surface channel") and shallow p–n-junctions about 10^{-5} cm in depth (Fig. 2).

In all cases, the specimens were doped with B to the concentration $p \sim 10^{15}$ cm^{-3} (a resistivity of about $5\,\Omega\cdot$cm, and the diffusion length of minority carriers $L_D \sim 20\div300$ μm).

Spectral characteristics were measured using a standard spectrometer SMP-3 at low light intensities of $10^{12}\div10^{14}$ quantum/(cm^2·s) in the visual and UV spectral ranges, and at higher intensities of $10^{14}\div10^{16}$ quantum/(cm^2·s) in the near-IR and visible spectral ranges.

3. Theoretical Analysis and Discussion

The spectral characteristics of the specimens of all types concerned are presented in Figs. 1 and 2 as functions of the wavelength λ and the absorption coefficient k. One can see that, in all cases, the photovoltage V_{SC} saturates within the λ-interval from 500 to 800 nm, which is typical of Si-based materials. The long-wave sides of the photovoltage spectra demonstrate a smooth recession. This fact makes it possible, using formula (1), to calculate the diffusion length of minority charge carriers, L_D, and determine the degree of its homogeneity over the surface.

The formula for V_{SC} normalized by the plateau value V_{SC}^m looks like [1–4]

$$V_{SC}(k) = V_{SC}^m \left[1 - \frac{\exp\left[-k\,L_{SC}\right]}{1 + k\,L_D} \right] = V_{SC}^m \frac{k\,L_D}{1 + k\,L_D}$$
(1a)

or

$$(V_{SC}/V^m)^{-1} = \frac{k\,L_D + 1}{1 + k\,L_D - \exp[-k, L_{SC}]} \approx$$

$$\approx 1 + 1/k\,L_D.$$
(1b)

The last relation gives the photovoltage dependence on the inverse scale.

Expression (1) is a generalized Gartner formula [1–3], which makes allowance for the bulk recombination and the recombination in the space charge region (SCR) in terms of the diffusion length $L_D = \sqrt{\tau D}$ and the SCR width L_{SC}. The influence of the additional recombination in the SCR is described by the negative term $-\exp(-k\,L_{SC})$, which diminishes the normalized photovoltage to 1 (its minimum value) not at $k_{-1} = 0$, but at a certain value determined
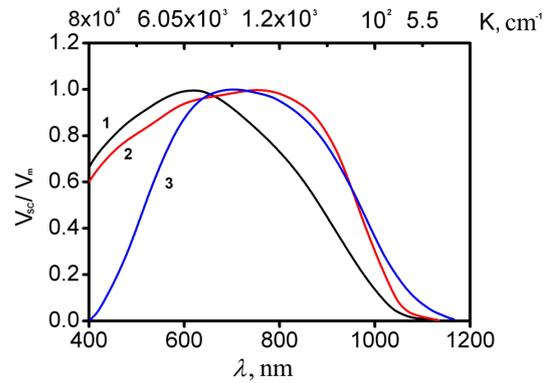
Fig. 1. Photovoltage spectra $V_{SC}(\lambda)$ for solar silicon wafers: real (chemically etched) surfaces (*1, 2*) and a surface implanted with Fe$^+$ ions (*3*)
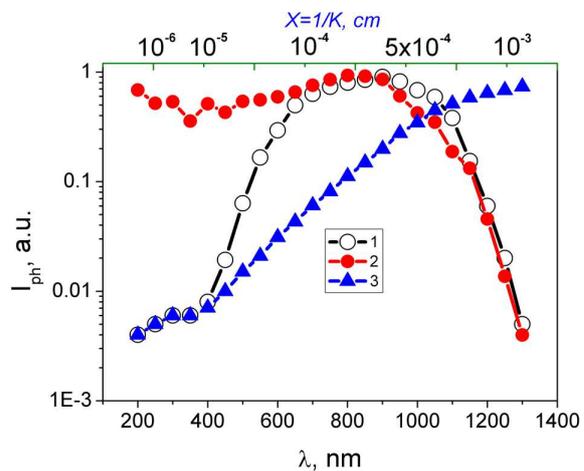

Fig. 2. Photocurrent spectra $I_{ph}(\lambda)$ for solar silicon specimens with barriers: diffusion-fabricated p–n-barrier (*1*), surface barrier SiO$_2$–Si (*2*). The spectrum of the inverse photocurrent $1/I_{ph}(1/k)$ for a diffusion solar cell with p–n-junction (*3*)

from the equation $\exp(-k\,L_{SC}) = k\,L_D$, as one can see from Fig. 3. Hence, those two formulas make it possible to determine the diffusion length and the screening width. For typical solar silicon, their values were obtained to equal $(2\div10)\times10^{-3}$ cm and $(0.1\div1)\times10^{-4}$ cm, respectively, which is in qualitative agreement with the results of electric measurements.

The rates of surface, S, and bulk, V_v, recombination were calculated next. They were determined, by using the formulas $S = D/L_{DS}$ (in the other approximation, $S \approx 1/k_s\tau_s$) and $V_v = D/L_D$, respectively. The surface diffusion length can be evaluated
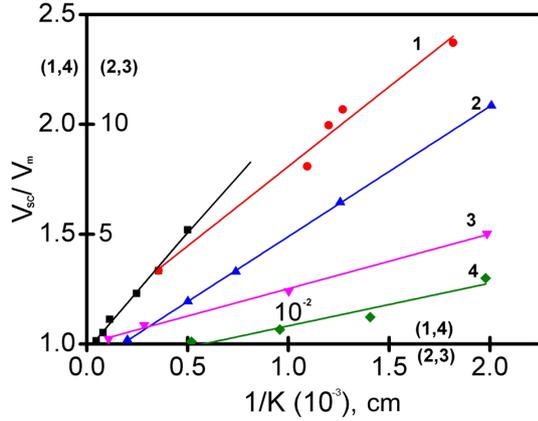
Fig. 3. Dependences of the inverse photovoltage on the inverse adsorption coefficient: Fe$^+$-implanted surfaces (*1* and *2*) and real (chemically etched) surfaces (*3* and *4*)

from the slope of the initial section of a decreasing interval in the right branch of the photovoltage spectrum, i.e. on the basis of the effective diffusion length $L_{\rm D}^*$ (Fig. 3):

$$1/L_{\rm D}^{2*} = 1/L_{\rm DV}^2 + 1/L_{\rm DS}^2.$$

Then, by analyzing curve *1* in Fig. 3, we obtained $S = 10^3$ cm/s and $V_v = 10^4$ cm/s. The bulk recombination also dominates in all other typical structures of solar silicon.

Now, let us consider the third, far short-wave, section of the photovoltage spectrum, where a considerable recession of the photovoltage is observed, as the excitation approaches the surface (Figs. 1 and 2). Here, the relation is also not obeyed, the recession is observed, and the saturation also takes place at the shortest wavelengths. Earlier, this section of the photovoltage spectrum was not analyzed because of the deficiency of experimental data.

One of the reasons for the photovoltage reduction at short waves can have a methodical character, namely, the violation of the linear (low-signal) regime,

$$V_{\rm SC} = {\rm const}\,\frac{\Delta n}{n_0}, \qquad (2)$$

when the surface barrier changes logarithmically,

$$V_{\rm SC} = {\rm const} \times \ln(1 + \exp[-Y_S]\,\Delta n/n_0). \qquad (3)$$

For the inverse barrier, the magnitude of $V_{\rm SC}$ can reach a maximum up to the energy gap value,

$$\Delta Y_S = 2U_{\rm B} - \ln\Delta_n \approx 2U_{\rm B} = {\rm const}. \qquad (4)$$

Such a barrier variation, as was marked above, can switch on new recombination-active levels and stimulate a drastic photovoltage drop. However, an effect with opposite action takes place simultaneously: the SCR field decreases in the reduced barrier, as well as the influence of recombination in the SCR. This regime with a change in the excitation level is typical of SC devices. But, when measuring the spectral characteristic $V_{\rm SC}(\lambda)$, the linear (low-signal) regime is retained.

Finally, let us consider an expression for the inverse photovoltage. Being written in terms of the inverse thickness of the region of excitation of nonequilibrium charge carriers, $x = 1/k(\lambda)$, it allows one to more conveniently distinguish different mechanisms of photovoltage spectrum formation at short waves:

$$\frac{V_{\rm SC}^m}{V_{\rm SC}(\lambda)} = C\,V_{\rm SC}^{-1} = C\,\frac{e}{kT}\,\frac{L_{\rm D}}{J_L}\,\frac{n_0(x)\,R_t(x)}{e^{-Y_s} - 1}, \qquad (5)$$

where

$$C = V_{\rm SC}^{\max} = \frac{kT}{e}\,J_L\,\frac{(q_S + 1)\,(e^{-Y_S} - 1)}{n_0^m\,R^m} \times$$
$$\times \left(1 - \frac{\exp(-k^m\,L_{\rm SC})}{1 + k^m L_{\rm D}}\right), \qquad (6)$$

$k(\lambda)$ is the experimentally determined function, $V_{\rm SC}^m$ is the plateau value in the dependence $V_{\rm SC}(\lambda)$, $R(x)$ the recombination rate, J_L the intensity of charge carrier generation per unit volume and unit time, $n_0(x)$ the equilibrium concentration of charge carriers in the bulk, $x = 1/k$ is the depth of the region of generation of charge carriers, $L_{\rm SC}$ the effective width of the surface space charge region (typically, $L_{\rm SC} \sim 10^{-5} \div 10^{-4}$ cm), k the light absorption coefficient, $L_{\rm D}$ the bulk diffusion length of excited carriers, and q_S the trap factor for photo-excited charge carriers.

The total recombination probability includes the recombination probabilities in the bulk, $1/\tau_v$, on the surface, $1/\tau_s = S/L_s$, and in the near-surface layer, $1/\tau_t(x)$:

$$R = \sum \frac{1}{\tau_i} = \frac{S}{L_{\rm D}} + \frac{1}{\tau_\nu} + \frac{1 + L_\tau^{\rm SC}}{\tau_t(x)}, \qquad (7)$$

where

$$L_- = \frac{I}{L_{\rm D}}\int_0^{L_{\rm SC}} \exp(-Y(x))dx, \qquad (8)$$

$$L_\tau^{\text{SC}} = \frac{\tau_\nu}{L_{\text{D}}} \int\limits_0^{L_{\text{SC}}} \exp(-Y(x))/\tau(x)dx, \qquad (9)$$

Y_S is the surface band bending in kT/e-units, L_τ^{SC} the factor of additional recombination in the SCR, and S the surface recombination rate, which is rather low ($S \sim 10^2 \div 10^3$ cm/s) in comparison with the bulk one, $V_v = 10^3 \div 10^4$.

Some of those quantities, e.g., n_0 and J_L, are independent of the measurement regime in the typical case of solar silicon, but the others depend on the device parameters. So, let us consider the following characteristics:

1) the surface recombination rate S,

2) $N_t(x)$ describing the doping in the near-surface region of the solar cell, which is determined by the specific fabrication technology,

3) L_τ^{SC}, which increases the magnitude of V_{SC} due to the SCR, and

4) technological factors such as mechanical and chemical treatments.

4. Analysis of Experimental Data and Discussion

Under typical conditions that solar silicon is subjected to, the following main recombination mechanisms govern the photovoltage parameters: the bulk recombination with the rate $V_v = L_{\text{D}}/\tau_v$, the surface recombination with the rate $S = \sqrt{D/\tau_s}$, and the recombination in the SCR with the rate L_-. At the depths $x > L_{\text{D}}$, we have $V_v = $ const, whereas S and L_- diminish to zero. However, near the surface, $\tau(x)$ can change owing to the SCR electric field and the charge carrier diffusion. This is a result of the mechanical stresses and the segregation and the diffusion of impurities (both implanted and intrinsic), which give rise to the generation/relaxation of various defects during technological treatments [10–12]. These processes also depend strongly on the initial material [13].

In a number of publications, those near-surface factors were combined into a phenomenologic surface recombination rate, which accepted unusually huge values (about $10^7 \div 10^9$ cm/s) at calculations [7,8]. More acceptable is a certain inhomogenetity near the surface, which arises owing to the distribution of additional recombination centers in the near-surface layer
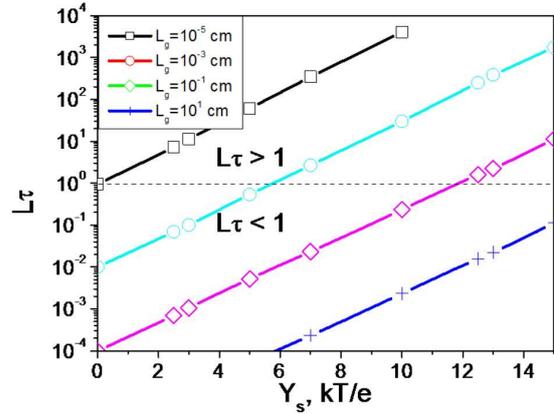

Fig. 4. Dependences of L_τ on the band bending Y_S for various diffusion lengths

and the influence of the SCR field [1–4, 9, 14]. Let us consider those factors in more details.

The recombination in the SCR is illustrated in Fig. 4. It becomes substantial when the band bending is large enough, $Y_{S0} > U_{\text{B}}$, where U_{B} is the Fermi energy in the bulk. This quantity was evaluated theoretically, by using formulas (8) and (9) (see Fig. 4). As was mentioned above, the illumination intensities $I \sim (0.1 \div 10)I_{\text{SOC}}$, which correspond to the injection levels $\Delta n = I_v \tau_v \sim 10^{15}$ cm^{-3}, are typical of SC devices. In other words, we have a nonlinear regime ($\Delta n/n_0 \sim 1$). Hence, under the typical conditions of solar cell operation, the recombination in the SCR is negligibly low (curve 1 in Fig. 3). As a result, for a typical solar silicon material and in the case of the photo-sensitive p–n-transition (the data are illustrated in Figs. 1, 2, and 5), the bulk recombination and the recombination in a narrow near-surface layer dominate, as a rule. The depth of the near-surface layer can even exceed the SCR width at that ($x \geqslant 3\ \mu$m).

Figure 5 exhibits the inverse photovoltage spectra as functions of the inverse coordinates for specimens of all analyzed types. The Fe-doped specimens demonstrate a moderate depletion with the band bending $_{S0} \sim -U_{\text{B}} \sim 7kT/e$ and the Fe distribution characterized by the density $N \approx 5 \times 10^{16}$ cm^{-2} and a penetration depth of about 10^{-5} cm, which is in qualitative agreement with calculations. A distribution "tail" of about 5×10^{-4} cm^{-2} is observed at deeper distances from the surface, which we associate with defects rapidly diffusing along the in-
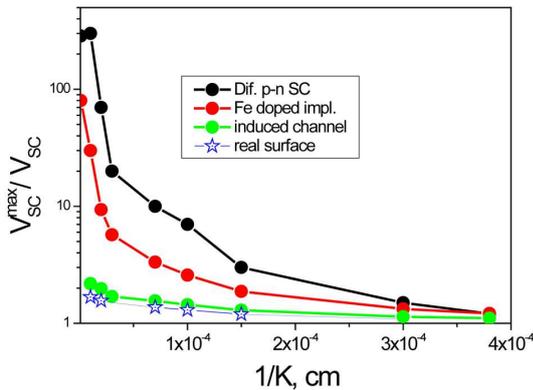
Fig. 5. Dependences of the inverse photovoltage $1/V_{SC}$ on the light absorption depth $1/k$ for specimens of various types

tergrain boundaries in the polycrystalline material [15–17].

Undoped specimens demonstrate a low depletion with the band bending $Y_{S0} \leqslant 7kT/e$. A small reduction of V_{SC} may be induced by the influence of surface impurities, which is typical of silicon oxidized at low temperatures [5].

Figure 5 also illustrates a drastic drop in the dependence of the inverse V_{SC} on the light penetration depth for a standard diffused p–n-junction. Namely, the V_{SC} signal decreases by more than two orders of magnitude in the short-wave region. A large drop at a distance of about 10^{-5} cm takes place owing to the surface recombination, the medium part of the drop is associated with the recombination in the developed SCR of the p–n-junction, and the long "tail" is a result of the disturbed part of the crystal volume localized near the surface of a device.

5. Conclusion

Using a generalized theory for the inverse photovoltage spectra, which involves a number of important factors such as the surface and bulk recombinations, diffusion length L_D, spatial distribution $N_t(x)$ of recombination centers near the surface, parameters of recombination in the SCR (the band bending Y_S and the SCR width), light adsorption coefficient k, and light adsorption depth $x = 1/k$, a method is proposed to calculate the electrical parameters of the silicon material and structures fabricated from solar silicon: thin-film structures, test device structures (MOS and with a diffusion channel), and ion-doped structures.

1. W. Gartner, Phys. Rev. **105**, 823 (1957).
2. V.A. Zuev and V.G. Litovchenko, Phys. Status Solidi B **16**, 751 (1966); V.A. Zuev, V.G. Litovchenko, and V.V. Antoshchuk, Surf. Sci. **32**, 365 (1972).
3. N.L. Dmitruk, Yu.V. Kryuchenko, V.G. Litovchenko, V.G. Popov, and M.A. Stepanova, Phys. Status Solidi A **124**, 183 (1991).
4. A.P. Gorban', V.G. Litovchenko, V.G. Popov, and A.A. Serba, Fiz. Tekh. Poluprovodn. **2**, 1400 (1977).
5. V.G. Litovchenko and A.P. Gorban', *Fundamentals of Physics of Metal-Insulator-Semiconductor Microelectronic Systems* (Naukova Dumka, Kyiv, 1978) (in Russian).
6. L. Kronik and Y. Shapira, Surf. Sci. Rep. **37**, 1 (1999).
7. A.P. Gorban', V.P. Kostylev, A.V. Sachenko, A.A. Serba, and V.V. Chernenko, Optoelektr. Poluprovodn. Tekhn. **37**, 61 (2002).
8. A.V. Sachenko, V.P. Kostylev, and V.G. Litovchenko, Ukr. J. Phys. **58**, 142 (2013).
9. V.G. Litovchenko, V.M. Naseka, and A.A. Evtukh, Ukr. J. Phys. **57**, 71 (2012).
10. D. Krüger, H. Rücker, B. Heinemann, V. Melnik, R. Kurps, and D. Bolze, J. Vac. Sci. Technol. B **22**, 455 (2004).
11. B. Romanjuk, V. Kladko, V. Melnik, V. Popov, V. Yukhymchuk, A. Gudymenko, Y. Olikh, G. Weidner, and D. Krüger, Mat. Sci. Semicond. Process. **8**, 171 (2005).
12. O. Oberemok, V. Kladko, V. Litovchenko, B. Romanyuk, V. Popov, V. Melnik, A. Sarikov, O. Gudymenko, and J. Vanhellemont, Semicond. Sci. Technol. **29**, 055008 (2014).
13. V.G. Litovchenko, B.M. Romanyuk, V.G. Popov, V.P. Melnik, O.S. Oberemok, V.P. Kladko, I.P. Lisovskyi, V.V. Strelchuk, V.V. Chernenko, and V.O. Shapovalov, Metallofiz. Noveish. Tekhnol. **33**, 873 (2011).
14. V.G. Litovchenko and V.M. Strikha, *Solar Power Industry: An Agenda for the World and Ukraine* (K.I.S., Kyiv, 2015) (in Ukrainian).
15. O. Korotchenko, A. Podolian, V. Kuryliuk, B. Romanyuk, V. Melnik, and I. Khatsevich, J. Appl. Phys. **111**, 063501 (2012).
16. O. Nichiporuk, A. Kaminski, M. Lemiti, A. Fave, S. Litvinenko, and V. Skryshevsky, Thin Solid Films **511–512**, 248 (2006).
17. O. Nichiporuk, A. Kaminski, M. Lemiti, A. Fave, and V. Skryshevsky, Sol. Energ. Mater. Sol. Cells **86**, 517 (2005).

В.Г. Литовченко

ДОСЛІДЖЕННЯ РЕКОМБІНАЦІЙНИХ
ПАРАМЕТРІВ СОНЯЧНОГО КРЕМНІЮ МЕТОДОМ
СПЕКТРОСКОПІЇ ПОВЕРХНЕВОЇ ФОТО-ЕРС

Р е з ю м е

Методом комбінованої поверхневої спектроскопії фото-ерс $V_{\rm sc}(\lambda)$ досліджено фундаментальні рекомбінаційні параметри фоточутливого сонячного кремнієвого матеріалу. Запропонований метод проаналізовано на прикладі 4-х типових кремнієвих структур: 1) пластини промислового фоточутливого кремнію з хімічно травленою (реальною) поверхнею; 2) структури з імплантованою рекомбінаційно-активною домішкою (Fe^+); 3) структури SiO_2–Si з фронтальним інверсним каналом; 4) структури з дифузійним p–n-переходом. Проведено порівняння з формулами для різних актуальних випадків, а саме для спектрів прямих та зворотних фото-ерс $V_{\rm SC}$, $1/V_{\rm SC}$ в координатах прямого та оберненого коефіцієнта поглинання k та $1/k$. Розраховано наступні рекомбінаційні характеристики сонячного кремнію: швидкості поверхневої та об'ємної рекомбінацій S та V; координаційна залежність приповерхневих рекомбінаційно-активних домішок та структурних технологічних домішок та дефектів в області приповерхневого просторового заряду.